

# Point process simulation of Generalised inverse Gaussian processes and estimation of the Jaeger Integral

Simon Godsill, Yaman Kindap  
SigProC Lab, University of Cambridge, UK

December 3, 2021

## Abstract

In this paper novel simulation methods are provided for the Generalised inverse Gaussian (GIG) Lévy process. Such processes are intractable for simulation except in certain special edge cases, since the Lévy density associated with the GIG process is expressed as an integral involving certain Bessel Functions, known as the Jaeger Integral in diffusive transport applications. We here show for the first time how to solve the problem indirectly, using generalised shot-noise methods to simulate the underlying point processes and constructing an auxiliary variables approach that avoids any direct calculation of the integrals involved. The augmented bivariate process is still intractable and so we propose a novel thinning method based on upper bounds on the intractable integrand. Moreover our approach leads to lower and upper bounds on the Jaeger integral itself, which may be compared with other approximation methods. We note that the GIG process is the required Brownian motion subordinator for the generalised hyperbolic (GH) Lévy process and so our simulation approach will straightforwardly extend also to the simulation of these intractable processes. Our new methods will find application in forward simulation of processes of GIG and GH type, in financial and engineering data, for example, as well as inference for states and parameters of stochastic processes driven by GIG and GH Lévy processes.

Keywords: Lévy Process, Generalised inverse Gaussian process, generalised hyperbolic process, diffusive transport, Jaeger integral, rejection sampling, Monte Carlo, Poisson point process, thinning

## 1 Introduction

The Lévy process is a fundamental tool for the study of continuous time stochastic phenomena [1]–[3]. The most familiar example is of course Brownian motion, but it is well known that the Gaussian assumption is inadequate for modelling of real-world phenomena, which are often more heavy-tailed than the Gaussian. Applications are found in areas such as financial modelling, [4]–[6] communications [7]–[12], signal processing [13], image analysis [14], [15] and audio processing [16], [17]. Non-Gaussian heavy-tailed effects are also important in the climatological sciences [18], [19], in the medical sciences [20] and for the understanding of sparse modelling/Compressive Sensing [21]–[29].

In this paper we study a very general class of non-Gaussian Lévy processes, the Generalised Inverse Gaussian process [2], [30], a process which can capture various degrees of heavy-tailed behaviour, including the gamma process, the inverse Gaussian and the reciprocal-gamma process, as well as processes that lie somewhere ‘in between’ these edge cases [30]. Our work also enables direct simulation of the mean-variance mixtures of GIG processes, leading to the Generalised Hyperbolic (GH) processes [31]. Important sub-classes of the GH process include the asymmetric Student-t process which has previously been intractable for simulation and inference to our knowledge (this class is entirely distinct from the Student-t processes developed in the Machine Learning literature [32]).

Rosinski [33] presents a generalised shot-noise representation of non-Gaussian Lévy processes, and it is this approach that we develop here for the GIG and GH processes. Our previous work using the shot noise representation has focussed on stable law processes and their applications in engineering, see [34]–[36] and references therein. There have been relevant developments in various special cases over recent years, including [37] who present the theory of normal-inverse Gaussian (NIG) processes, [38] who present approximate sampling methods for the NIG case, while [39] give applications of series based methods for non-Gaussian Ornstein-Uhlenbeck (OU) processes. [40] provided rejection sampling and series based simulations for the GIG OU process using the concepts of [33], but these are applied to a different Background driving Lévy process (BDLP) than our work and indeed require evaluation of

a generally intractable integral involving Bessel Functions. In addition [41], [42] have provided exact simulation methods for the related class of tempered stable (TS) processes.

The distribution of the GIG Lévy process at  $t = 1$ , the GIG distribution, possesses a three parameter probability density function defined for positive real random variables as follows [30]:

$$f_{GIG}(x) = \left(\frac{\gamma}{\delta}\right)^\lambda \frac{1}{2K_\lambda(\delta\gamma)} x^{\lambda-1} e^{-\frac{1}{2}(\delta^2 x^{-1} + \gamma^2 x)} \mathcal{I}_{x>0} \quad (1)$$

where  $\lambda \in \mathbb{R}$ ,  $K_\lambda(\cdot)$  is the modified Bessel function of the second kind and  $\mathcal{I}$  is the indicator function. The support of parameters  $\gamma$  and  $\delta$  depend on the sign of  $\lambda$  as discussed in [30]. It is shown in [43] that the GIG distribution is infinitely divisible and hence can be the distribution of a Lévy process at time  $t = 1$ . Furthermore, particular values of the parameters lead to special cases of the GIG distribution such as the Inverse Gaussian ( $\lambda = -1/2$ ), Gamma ( $\delta = 0$ ,  $\lambda > 0$ ) and the Reciprocal-Gamma ( $\gamma = 0$ ,  $\lambda < 0$ ) distributions, and in these limit cases the normalising constant is adjusted to the normalising constant of these well known distributions.

The principal contribution of this paper is to provide a comprehensive suite of methods for simulation of GIG processes, without the need for evaluation of intractable integrals, beyond pointwise evaluation of the relevant Bessel functions. An auxiliary variables approach transforms the univariate GIG point process into a bivariate point process having the GIG process as its marginal by construction, and requiring no explicit evaluation of integrals. We derive tractable dominating measures for the augmented GIG Lévy density, hence leading to a random thinning methodology for generation of jumps of the underlying marginal GIG process. The whole procedure is carried out through generation of familiar random variables (from the gamma family) and point processes (both gamma and tempered stable). In addition we are able to bound the average acceptance rates of the random variate generation and also to provide upper and lower bounds on the GIG Lévy density and the corresponding Jaeger integral. Finally the whole methodology is made accessible to practitioners through the publication of Matlab and Python code to implement the GIG sampling schemes.

Section 2 presents the necessary preliminaries for simulation of Lévy processes and their corresponding point processes, using a generalised shot-noise approach. Section 3 gives the specific forms for the GIG Lévy density and derives bounds on these densities, as well as a generic thinning method for tractable sampling of the underlying point processes, and presents in detail the simulation method for two different parameter ranges of the process. Section 4 presents example simulations, compared with exact simulations of the GIG random variable and finally Section 5 discusses the application of GIG processes in simulation and inference for more general processes including the Generalised Hyperbolic Process.

## 2 Shot noise representations, Lévy densities and thinning

In this section we present the required preliminaries about Lévy processes and shot-noise simulation of those processes, using the framework of [33]. The characteristic function for a general non-negative-valued Lévy process having no drift or Brownian motion part is given by [44], Corollary 15.8, as:

$$E[\exp(iuW(t))] = \exp t \left[ \int_{(0,\infty)} (e^{iuw} - 1 - iuw\mathcal{I}_{|w|\leq 1})Q(dw) \right] \quad (2)$$

where  $Q$  is a Lévy measure on  $(0, \infty)$ . By the Lévy-Ito integral representation, we may express  $W(t)$  directly as:

$$W(t) = \int_{|w|\leq 1} w[(N([0, t], dw) - tQ(dw))] + \int_{|w|>1} wN([0, t], dw) \quad (3)$$

Here  $N$  is a bivariate point process having mean measure *Lebesgue*  $\times$   $Q$  on  $[0, T] \times (0, \infty)$ , which can be conveniently expressed as:

$$N = \sum_{i=1}^{\infty} \delta_{V_i, J_i}$$

where  $\{V_i \in [0, T]\}$  are i.i.d. uniform random variables which give the times of arrival of jumps,  $\{J_i\}$  are the size of the jumps and  $\delta_{V_i, J_i}$  is the Dirac measure centered at time  $V$  and jump size  $J$ .

Substituting  $N$  directly into (3) leads to

$$W(t) = \sum_{i=1}^{\infty} J_i \mathcal{I}_{V_i \leq t} - tc_i, \text{ as}$$

where  $c_i$  are compensator terms, which may be taken as zero for the cases considered in this paper. The almost sure convergence of this series to  $\{W(t)\}$  is proven in [33].

In principle it may be possible to simulate directly from the point process  $N$ , but in practice the potentially infinite number of jumps in any finite time interval make this impossible. If the jumps can be ordered by size, however, it may be possible to simulate all of the significant jumps and ignore or approximate the residual error from omitting the smallest jumps. It turns out that this can be done in a very convenient way, using the well known approach of [33], [45]. The starting point is the simulation of the epochs of a unit rate Poisson process  $\{\Gamma_i\}_{i \geq 1}$ . The intensity function of this process is of course  $\lambda_{\Gamma} = 1$ , and the resulting realisations contain almost surely an infinite number of terms. We know how to simulate an arbitrarily large number of ordered terms from this process by repeatedly generating exponential random variables and calculating the cumulative sum of these to obtain an ordered  $\Gamma_i$  sequence. Now take a deterministic, non-increasing function  $h(\Gamma)$  of the epochs to obtain a transformed point process:

$$N' = \sum_{i=1}^{\infty} \delta_{V_i, h(\Gamma_i)}$$

then we would like this process to be equivalent to the original point process  $N$ . Suppose that the Lévy measure for  $N$  is  $Q(\cdot)$ , defined for positive support  $J \in (0, \infty)$  then we can determine the appropriate function  $h(\cdot)$  to obtain the correct point process  $N$ . This is straightforward to achieve. Note that for all  $\gamma \in [0, \infty)$ ,

$$E[\#\{J_i; J_i \geq j\}] = h^{-1}(j)$$

But for the point process  $N$  it is required that  $E[\#\{J_i; J_i \geq j\}] = Q([j, \infty)) = Q^+(j)$  where  $Q^+(j)$  is defined as the upper tail probability of the Lévy measure. So, finally,

$$h(\gamma) = Q^{+-1}(\gamma)$$

where  $Q^{+-1}(\cdot)$  is the inverse of the upper tail probability of the Lévy measure. This is a well known result, proposed for simulation of Lévy processes by many authors including [33], [45]. Thus, to generate points directly from  $N$  by this method it is necessary to be able to compute  $Q^{+-1}(\cdot)$  explicitly, either in closed form or by numerical approximations. In some cases where this is not possible it may nevertheless be possible to simulate directly from a bounding process  $N_0$  with  $dQ_0(x)/dQ(x) \geq 1 \forall x \in (0, \infty)$  and then to thin with probability  $dQ(x)/dQ_0(x)$  in order to obtain samples from  $N$  [46]. In all cases considered here the Lévy measure possesses a density function, which we also denote by  $Q(x)$  (using the minor abuse of notation ‘ $dQ(x) = Q(x)dx$ ’) and the required bounding condition is then  $Q_0(x) \geq Q(x)$ , with associated thinning probability  $Q(x)/Q_0(x)$ .

Simulation examples required for this paper are the tempered stable (TS) and gamma processes, which may be sampled as follows:

## 2.1 Tempered stable point process

In the tempered stable (TS) case the Lévy density is, for  $\alpha \in (0, 2)$  [47] (see also [48])

$$Q(x) = Cx^{-1-\alpha}e^{-\beta x}$$

The tail probability may be calculated in terms of gamma functions, but is not easily inverted. Instead it may be split into a positive  $\alpha$ -stable process [49] with density  $Q_0(x) = Cx^{-1-\alpha}$  and a tempering function  $e^{-\beta x}$ . The stable law process has tail mass  $Q_0^+(x) = \frac{C}{\alpha}x^{-\alpha}$  and hence  $h(\gamma) = Q_0^+(\gamma)^{-1} = (\frac{\alpha\gamma}{C})^{-1/\alpha}$  [49]. Having simulated the point process with rate function  $Q_0$ , points are individually selected (thinned) with probability  $e^{-\beta x}$ , otherwise deleted.

## 2.2 Gamma process

The Lévy density for the Gamma process is:

$$Q(x) = Cx^{-1}e^{-\beta x}$$

[33] suggests four possible sampling schemes for this process. The tail probability is the Exponential integral, which would require numerical inversion, see [50]. Instead we adopt the thinning (also called the ‘rejection method’ in [33]) version of this in which a dominating point process is chosen as  $Q_0(x) = \frac{C}{x}(1 + \beta x)^{-1}$ . The tail probability for this is  $Q_0^+(x) = C \log(\beta^{-1}x^{-1} + 1)$  and hence  $h(\gamma) = \frac{1}{\beta(\exp(\gamma/C) - 1)}$ . Points are then thinned with probability  $(1 + \beta x) \exp(-\beta x) \leq 1$ . As reported in [33], this thinning method is highly effective, with very few point rejections observed.

## 3 Simulation from the Generalised inverse Gaussian Lévy process

In this section the GIG Lévy density is presented and a general scheme is presented that will enable simulation from the GIG process.

The Lévy density for the Generalised inverse Gaussian (GIG) process is given by [30]:

$$\frac{e^{-x\gamma^2/2}}{x} \left[ \int_0^\infty \frac{e^{-xy}}{\pi^2 y |H_{|\lambda|}(\delta\sqrt{2y})|^2} dy + \max(0, \lambda) \right], \quad x > 0$$

where  $H_\lambda(z) = J_\lambda(z) + iY_\lambda(z)$  is the Bessel function of the third kind, also known as the Hankel function,  $J_\lambda(z)$  is the Bessel function of the first kind, and  $Y_\lambda(z)$  is the Bessel function of the second kind.

The GIG Lévy density comprises two terms: the initial integral, which we denote  $Q_{GIG}(x)$ :

$$Q_{GIG}(x) = \frac{e^{-x\gamma^2/2}}{x} \int_0^\infty \frac{e^{-xy}}{\pi^2 y |H_{|\lambda|}(\delta\sqrt{2y})|^2} dy, \quad x > 0$$

added to a second term, present only for  $\lambda > 0$ :

$$\frac{e^{-x\gamma^2/2}}{x} \max(0, \lambda), \quad x > 0$$

This second term is a Gamma process that may be straightforwardly simulated using the standard methods of 2.2 and added to the simulation of points from the first term  $Q_{GIG}(x)$ . Hence we will neglect this second term for now. It will be convenient to rewrite  $Q_{GIG}(x)$  using the substitution  $z = \delta\sqrt{2y}$  as:

$$Q_{GIG}(x) = \frac{e^{-x\gamma^2/2}}{x} \int_0^\infty \frac{e^{-xy}}{\pi^2 y |H_{|\lambda|}(\delta\sqrt{2y})|^2} dy = \frac{2e^{-x\gamma^2/2}}{\pi^2 x} \int_0^\infty \frac{e^{-\frac{z^2 x}{2\delta^2}}}{z |H_{|\lambda|}(z)|^2} dz$$

Note that this integral is known elsewhere as the Jaeger Integral, which finds application in diffusive transport [51]. Beyond our direct interest in GIG processes, there is significant interest in approximating these integrals accurately, and our bounding approach is likely to provide accurate bounds and approximations which may be compared with those proposed in [51].

Throughout this paper we will consider only positive and real-valued variables  $x, y$  and  $z$ , as the complex versions of these functions are not required in the present context.

Our general scheme is to consider the following bivariate point process on  $(0, \infty) \times (0, \infty)$ :

$$Q_{GIG}(x, z) = \frac{2e^{-x\gamma^2/2}}{\pi^2 x} \frac{e^{-\frac{z^2 x}{2\delta^2}}}{z |H_{|\lambda|}(z)|^2} \tag{4}$$

which has by construction the GIG process as its marginal:

$$Q_{GIG}(x) = \int_0^\infty Q_{GIG}(x, z) dz$$

We propose to simulate points directly from this bivariate process, hence avoiding any direct evaluation of the Jaeger Integral. Since  $Q_{GIG}(x, z)$  is intractable itself for simulation, dominating processes  $Q_{GIG}^0(x, z) \geq Q_{GIG}(x, z)$  are constructed and points sampled from  $Q_{GIG}^0(x, z)$  are thinned with probability  $Q_{GIG}(x, z)/Q_{GIG}^0(x, z)$ . Thus a significant part of our approach is in constructing suitable dominating functions that are tractable for simulation, and this is achieved by studying the properties of the Jaeger Integral.

The first set of bounds is obtained from the basic properties of the Hankel function [52] and will lead in particular to a simulation algorithm for the case  $|\lambda| \geq 0.5$ :

**Theorem 3.1.** *For  $|\lambda| \geq 0.5$ , the following bound applies:*

$$Q_{GIG}(x, z) \leq \frac{e^{-x\gamma^2/2}}{\pi x} e^{-\frac{z^2 x}{2\delta^2}} \quad (5)$$

and, for  $|\lambda| \leq 0.5$ ,

$$Q_{GIG}(x, z) \geq \frac{e^{-x\gamma^2/2}}{\pi x} e^{-\frac{z^2 x}{2\delta^2}} \quad (6)$$

*Proof.* We have an asymptotic expansion for  $|H_\nu(z)|^2$  ([52], Section 13.75):

$$|H_\nu(z)|^2 \sim \frac{2}{\pi z} \sum_{m=0}^{\infty} \{1 \times 3 \dots \times (2m-1)\} \frac{(v, m)}{2^m z^{2m}}$$

where  $(\nu, m)$  is defined as ([52], Section 13.75) sec. 7.2 p. 198):

$$(v, m) = \frac{\Gamma(\nu + m + 1/2)}{m! \Gamma(\nu - m + 1/2)} = \frac{\{4\nu^2 - 1^2\} \{4\nu^2 - 3^2\} \dots \{4\nu^2 - (2m-1)^2\}}{2^{2m} m!}$$

so that in particular we have:

$$\begin{aligned} (\nu, 0) &= 1 \\ (\nu, 1) &= \frac{(4\nu^2 - 1)}{4} = \begin{cases} < 0, & \nu < 0.5 \\ > 0, & \nu > 0.5 \end{cases} \\ (\nu, 2) &= \frac{(4\nu^2 - 1)(4\nu^2 - 9)}{2^5} = \begin{cases} > 0, & \nu < 0.5 \\ < 0, & \nu > 0.5 \end{cases} \end{aligned}$$

Moreover, when  $p > \nu - 1/2$ , the remainder after  $p$  terms ‘have the same sign as, and numerically less than, the  $(p+1)$ th term’ ([52], Section 13.75). Thus,

$$|H_\nu(z)|^2 \sim \frac{2}{\pi z} \left( 1 + \frac{4\nu^2 - 1}{8z^2} + \frac{3(4\nu^2 - 1)(4\nu^2 - 9)}{2^7 z^4} + O(z^{-6}) \right)$$

Using a truncated version of the asymptotic expansion, we find the following lower bounds:

$$|H_\nu(z)|^2 \geq \begin{cases} \frac{2}{\pi z}, & \nu \geq 0.5 \\ \frac{2}{\pi z} \left( 1 + \frac{(4\nu^2 - 1)}{8z^2} \right), & \nu < 0.5 \end{cases} \quad (7)$$

and the following upper bound for  $\nu \leq 0.5$ :

$$|H_\nu(z)|^2 \leq \frac{2}{\pi z} \quad (8)$$

The results follow by substitution of (7) and (8) into  $Q_{GIG}(x, z)$  (4).  $\square$

**Corollary 3.1.1.** *The bound in (5), applicable for  $|\lambda| \geq 0.5$ , can be rewritten as*

$$\frac{e^{-x\gamma^2/2}}{\pi x} e^{-\frac{z^2 x}{2\delta^2}} = \frac{\delta\Gamma(1/2)e^{-x\gamma^2/2}}{\sqrt{2\pi}x^{3/2}} \sqrt{Ga} \left( z|1/2, \frac{x}{2\delta^2} \right) \quad (9)$$

where  $\sqrt{Ga}$  is the square-root gamma density, i.e. the density of  $X^{0.5}$  when  $X \sim Ga(\alpha, \beta)$ , having probability density function

$$\sqrt{Ga}(\alpha, \beta) = \frac{2\beta^\alpha}{\Gamma(\alpha)} x^{2\alpha-1} e^{-\beta x^2}$$

It can be seen immediately that (9) corresponds marginally to a tempered stable process in  $x$ , and conditionally to a  $\sqrt{Ga}$  density for  $z$ , a tractable feature that will enable sampling from the dominating bivariate point process.

Integration wrt  $z$  leads to a simple upper bound on the GIG Lévy density:

$$\frac{\delta\Gamma(1/2)e^{-x\gamma^2/2}}{\sqrt{2\pi}x^{3/2}} \quad (10)$$

which was also obtained by [40], and used in a rejection sampling procedure that requires a direct evaluation of the Jaeger integral, in contrast with our approach. For  $|\lambda| \leq 0.5$ , a similar argument leads to a lower bound with the same formula as (10).

**Remark.** The first bound for  $\nu \geq 0.5$  in (7) will be used shortly as an envelope function for rejection sampling in the case  $|\lambda| \geq 0.5$  using Corollary 3.1.1. However, the second bound in (7) for  $|\lambda| < 0.5$  would lead to an improper envelope function that is not integrable wrt  $z$ , hence we will need to develop more sophisticated bounds for the case  $|\lambda| < 0.5$ .

A second set of bounds can be stated as follows.

**Theorem 3.2.** Choose a point  $z_0 \in (0, \infty)$  and compute  $H_0 = z_0|H_\nu(z_0)|^2$ . This will define the corner point on a piecewise lower or upper bound. Define now  $z_1 = \left( \frac{2^{1-2\nu}\pi}{\Gamma^2(\nu)} \right)^{1/(1-2\nu)}$  and define the following functions:

$$A(z) = \begin{cases} z(\Gamma(\nu)/\pi)^2 \left( \frac{2}{z} \right)^{2\nu}, & z < z_1 \\ \frac{2}{\pi}, & z \geq z_1 \end{cases}$$

and

$$B(z) = \begin{cases} H_0 \left( \frac{z_0}{z} \right)^{2\nu-1}, & z < z_0 \\ H_0, & z \geq z_0 \end{cases}$$

Then, for  $0 < \nu \leq 0.5$ ,

$$A(z) \geq z|H_\nu(z)|^2 \geq B(z) \quad (11)$$

and for  $\nu \geq 0.5$ ,

$$A(z) \leq z|H_\nu(z)|^2 \leq B(z) \quad (12)$$

with all inequalities becoming equalities when  $\nu = 0.5$ , and both  $A(z)$  bounds (left side inequalities) becoming tight at  $z = 0$  and  $z = \infty$ .

*Proof.* First note that  $z|H_\nu(z)|^2$  is an increasing function for  $0 < \nu < 0.5$  and decreasing for  $\nu > 0.5$  ([52], Section 13.75). When combined with the tight bound of  $2/\pi$  as  $z \rightarrow \infty$  (7) this leads directly to the  $2/\pi$  components of  $A(z)$ . Similarly the first part of the bound  $A(z)$ ,  $z(\Gamma(\nu)/\pi)^2 \left( \frac{2}{z} \right)^{2\nu}$ , is justified since [51] proves that  $z^{2\nu}|H_\nu(z)|^2$  is increasing when  $\nu > 0.5$  and decreasing when  $\nu < 0.5$ , with a tight bound of  $(\Gamma(\nu)/\pi)^2 2^{2\nu}$  as  $z \rightarrow 0$ . Thus the left hand side of the inequalities,  $A(z)$ , are established.

The right hand side of the inequalities,  $B(z)$ , are proven by the monotonicity and sign of gradient for both  $z^{2\nu}|H_\nu(z)|^2$  and  $z|H_\nu(z)|^2$ . We may choose an arbitrary corner point  $(z_0, H_0)$  on  $z|H_\nu(z)|^2$  and monotonicity of  $z|H_\nu(z)|^2$  immediately implies that

$$z|H_\nu(z)|^2 \begin{cases} \geq H_0, & 0 < \nu \leq 0.5 \\ \leq H_0, & \nu \geq 0.5 \end{cases}$$

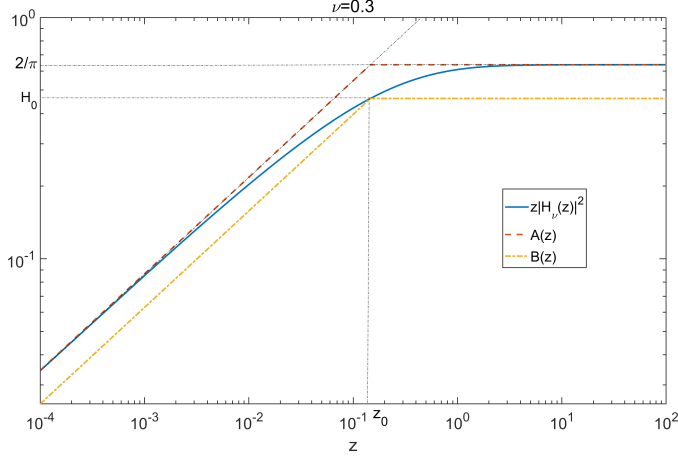


Figure 1: Plot of Bessel function bounds,  $\nu = 0.3$ .  $z_0$  set equal to  $z_1$ .

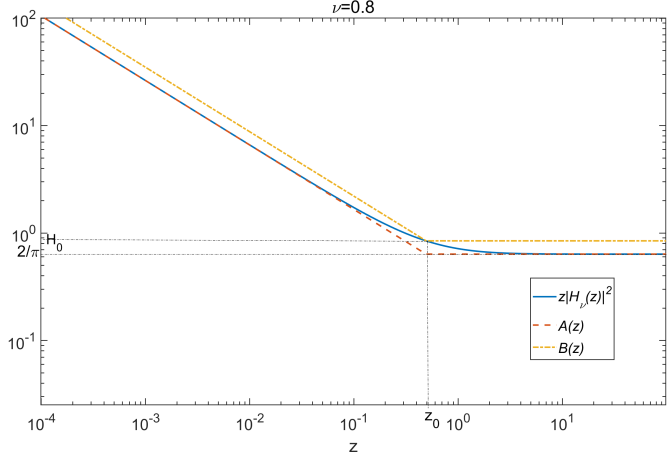


Figure 2: Plot of Bessel function bounds,  $\nu = 0.8$ .  $z_0$  set equal to  $z_1$ .

Moreover, monotonicity and sign of gradient of  $z^{2\nu}|H_\nu(z)|^2$  [51] imply that

$$z^{2\nu}|H_\nu(z)|^2 \begin{cases} \geq z^{2\nu-1}H_0, & 0 < \nu \leq 0.5 \\ \leq z^{2\nu-1}H_0, & \nu \geq 0.5 \end{cases}$$

from which the bounds  $B(z)$  are immediately obtained.  $\square$

**Remark.** The proven bounds can be clearly visualised on a log-log plot, which highlights the asymptotic behaviour of the functions and bounds as  $z \rightarrow 0$  and  $z \rightarrow \infty$ , see Figs. 1 and 2.

**Remark.** The choice of  $z_0 \in (0, \infty)$  is arbitrary. However, its value will impact the tightness of the bounding functions  $B(z)$  and will hence impact the effectiveness of our subsequent sampling algorithms and integral approximations. A suitable generic choice was found to be at the same  $z$  value as the corner point of the corresponding  $A(z)$  bounds, i.e. set  $z_0 = z_1$ , as plotted in Figs. 1 and 2, though further optimisation may be possible in applications.

**Corollary 3.2.1.** For the case  $|\lambda| < 0.5$ , the right hand bound in (11),  $B(z)$ , can be substituted into  $Q_{GIG}(x, z)$  (4)

and rearranged to obtain:

$$\begin{aligned}
Q_{GIG}(x, z) &= \frac{2e^{-x\gamma^2/2}}{\pi^2 x} \frac{e^{-\frac{z^2 x}{2\delta^2}}}{z|H_{|\lambda|}(z)|^2} \leq \frac{e^{-x\gamma^2/2}}{\pi^2 x} \begin{cases} \frac{z^{2|\lambda|-1} e^{-\frac{z^2 x}{2\delta^2}}}{H_0 z_0^{2|\lambda|-1}}, & 0 < z < z_0 \\ \frac{e^{-\frac{z^2 x}{\delta^2}}}{H_0}, & \text{otherwise} \end{cases} \\
&= \frac{e^{-x\gamma^2/2}}{\pi^2 x^{1+|\lambda|}} \frac{(2\delta^2)^{|\lambda|} \gamma(|\lambda|, z_0^2 x / (2\delta^2)) \frac{\Gamma(|\lambda|) \sqrt{Ga}(z||\lambda|, x/(2\delta^2))}{\gamma(|\lambda|, z_0^2 x / (2\delta^2))}}{H_0 z_0^{2|\lambda|-1}} \mathcal{I}_{0 < z < z_0} \\
&\quad + \frac{e^{-x\gamma^2/2}}{\pi^2 x^{3/2}} \frac{(2\delta^2)^{0.5} \Gamma(0.5, z_0^2 x / (2\delta^2)) \frac{\Gamma(0.5) \sqrt{Ga}(z|0.5, x/(2\delta^2))}{\Gamma(0.5, z_0^2 x / (2\delta^2))}}{H_0} \mathcal{I}_{z \geq z_0} \quad (13)
\end{aligned}$$

This can be split up into a two tractable point processes for simulation: a first,  $N_1$ , comprising a modified tempered  $|\lambda|$ -stable process with truncated  $\sqrt{Ga}$  conditional for  $z$ , and a second,  $N_2$ , comprising a modified tempered 0.5-stable process with a further truncated  $\sqrt{Ga}$  conditional for  $z$ . We will use this union of point processes as the dominating Lévy measure in simulation of the  $|\lambda| < 0.5$  case.

**Corollary 3.2.2.** *Integration of the bounding function (13) wrt  $z$  allows a more sophisticated estimate for the Jaeger integral and therefore the Lévy density for the GIG process, which is an upper bound for  $|\lambda| < 0.5$  and a lower bound for  $|\lambda| > 0.5$ , following the direction of the right hand inequalities in (13) and (12). A similar procedure inserting the left hand ( $A(z)$ ) inequalities from (13) and (12) yields the corresponding lower ( $|\lambda| < 0.5$ ) and upper ( $|\lambda| > 0.5$ ) bounds. Define first the bounding functions  $Q_{GIG}^A(x)$  and  $Q_{GIG}^B(x)$ , corresponding to the bounds  $A(z)$  and  $B(z)$  as follows:*

$$\begin{aligned}
Q_{GIG}^A(x) &= \frac{e^{-x\gamma^2/2}}{\pi x^{1+|\lambda|}} \frac{(2\delta^2)^{|\lambda|} \gamma(|\lambda|, z_1^2 x / (2\delta^2))}{2z_1^{2|\lambda|-1}} + \frac{e^{-x\gamma^2/2}}{\pi x^{3/2}} \frac{(2\delta^2)^{0.5} \Gamma(0.5, z_1^2 x / (2\delta^2))}{2} \\
Q_{GIG}^B(x) &= \frac{e^{-x\gamma^2/2}}{\pi^2 x^{1+|\lambda|}} \frac{(2\delta^2)^{|\lambda|} \gamma(|\lambda|, z_0^2 x / (2\delta^2))}{H_0 z_0^{2|\lambda|-1}} + \frac{e^{-x\gamma^2/2}}{\pi^2 x^{3/2}} \frac{(2\delta^2)^{0.5} \Gamma(0.5, z_0^2 x / (2\delta^2))}{H_0}
\end{aligned}$$

These are obtained by substituting the bounds  $A(z)$  or  $B(z)$  into the expression for  $Q_{GIG}(x, z)$  (4) and integrating wrt  $z$ .

Noting that  $z_0 \in (0, \infty)$  can be chosen arbitrarily, the  $Q_{GIG}^B$  estimates may be improved by optimising wrt  $z_0$  to either maximise ( $|\lambda| < 0.5$ ) or minimise ( $|\lambda| > 0.5$ )  $Q_{GIG}^B(x)$  at each point  $x$ .

Then, following the direction of the inequalities in (11) and (12) we obtain the following estimates of  $Q_{GIG}(x)$ :

$$\begin{aligned}
Q_{GIG}^A(x) &\leq Q_{GIG}(x) \leq \min_{z_0 \in (0, \infty)} \{Q_{GIG}^B(x)\}, \quad |\lambda| \leq 0.5 \\
Q_{GIG}^A(x) &\geq Q_{GIG}(x) \geq \max_{z_0 \in (0, \infty)} \{Q_{GIG}^B(x)\}, \quad |\lambda| \geq 0.5
\end{aligned}$$

with all inequalities becoming equalities at  $|\lambda| = 0.5$ . Optimisation to achieve the required maximum and minimum functions can be achieved by numerical search.

Example plots are given in Fig. 3 in which the optimised lower and upper bounds are plotted, showing very close agreement (often indistinguishable by eye) in their estimation of  $Q_{GIG}(x)$ , over various parameter ranges and large  $x$  ranges (i.e. the bounds are visually quite tight). Overlaid are the  $x^{-3/2}$  and  $x^{-(1+|\lambda|)}$  trends and also the simple approximation of (10). This simple approximation diverges significantly from our proposed bounds, particularly when  $|\lambda|$  is not close to 0.5 (when  $|\lambda| = 0.5$  all bounds are equal to the true function  $Q_{GIG}(x)$  for the Inverse Gaussian (IG) process).

### 3.1 Simulation of GIG processes with $|\lambda| \geq 0.5$

In this section the specific algorithm applied for simulation in the case  $|\lambda| \geq 0.5$  is detailed. In this parameter range it has been found very effective to use Theorem 3.1 and Corollary 3.1.1, so that the dominating bivariate process is:

$$Q_{GIG}^0(x, z) = \frac{e^{-x\gamma^2/2}}{\pi x} e^{-(z^2 x) / (2\delta^2)}$$

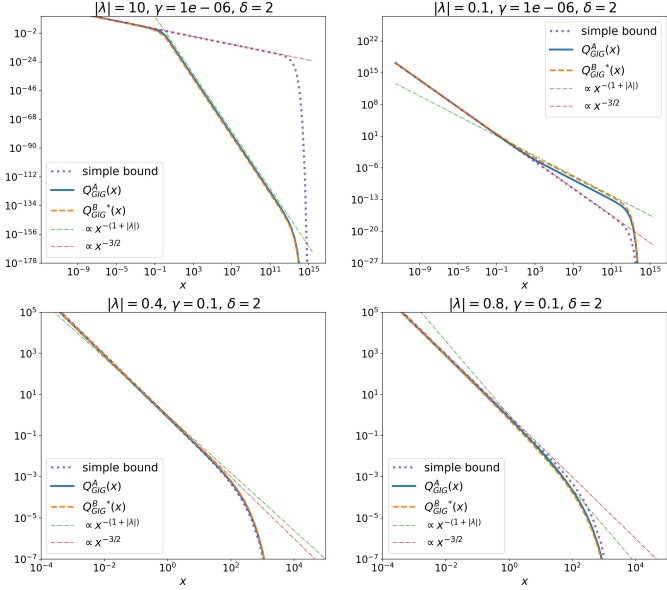


Figure 3: Plot of optimised upper and lower bounds on  $Q_{GIG}(x)$ , for various parameter settings. We use the following shorthand for the optimised  $Q^B$  bounds:  $Q_{GIG}^{B*}(x) = \max_{z_0 \in (0, \infty)} \{Q_{GIG}^B(x)\}$ , where min applies for  $|\lambda| < 0.5$  and max applies for  $|\lambda| \geq 0.5$ . Overlaid also are the simple approximation (7) and the trends  $x^{-3/2}$  and  $x^{-(1+|\lambda|)}$ .

The thinning probability for points drawn from the dominating point process is then:

$$\frac{Q_{GIG}(x, z)}{Q_{GIG}^0(x, z)} = \frac{2}{\pi z |H_{|\lambda|}(z)|^2}$$

The recipe for generation of points from the bivariate point process is:

1. Generate a large number of points from the tempered stable process with intensity function, sorted large to small using a shot noise series:

$$\frac{e^{-x\gamma^2/2}}{x^{3/2}} \frac{\delta\Gamma(1/2)}{\sqrt{2\pi}}$$

2. For each point  $x$ , draw a random variate  $z \sim \sqrt{\text{Ga}}(z|1/2, x/(2\delta^2))$

3. Accept with probability

$$\frac{2}{\pi z |H_{|\lambda|}(z)|^2}$$

### 3.1.1 Acceptance rate

The mean acceptance probability for fixed  $x$  is:

$$\rho(x) = E \left[ \frac{2}{\pi z |H_{|\lambda|}(z)|^2} \right] = \int_0^\infty \sqrt{\text{Ga}}(z|1/2, x/(2\delta^2)) \frac{2}{\pi z |H_{|\lambda|}(z)|^2} dz$$

which may be bounded using Theorem 3.2. For the current parameter setting ( $|\lambda| > 0.5$ ) we have  $A(z) \leq z |H_{|\lambda|}(z)|^2 \leq B(z)$ . Lower and upper bounds are obtained by substituting  $A(z)$  and  $B(z)$  and then by direct integration to give:

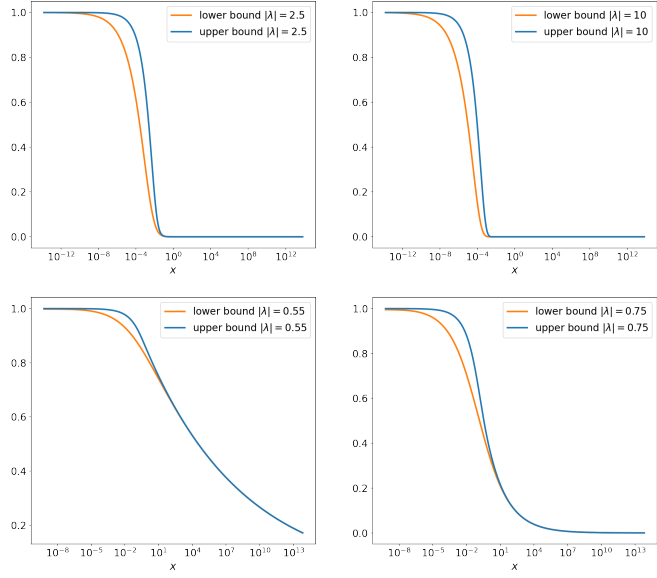


Figure 4: Plot of upper and optimised lower bounds on  $\rho(x)$ , for various  $|\lambda| > 0.5$ , showing that large jumps are rejected while with increasing probability small jumps are accepted.  $\delta = 0.1$  in all cases and bounds do not depend on  $\gamma$

$$\begin{aligned} \frac{2}{\pi H_0} \left( \left( \frac{z_0^2 x}{2\delta^2} \right)^{0.5-|\lambda|} \frac{\gamma(|\lambda|, z_0^2 x / (2\delta^2))}{\Gamma(0.5)} + \frac{\Gamma(0.5, z_0^2 x / (2\delta^2))}{\Gamma(0.5)} \right) \\ \leq \rho(x) \leq \left( \frac{z_1^2 x}{2\delta^2} \right)^{0.5-|\lambda|} \frac{\gamma(|\lambda|, z_1^2 x / (2\delta^2))}{\Gamma(0.5)} + \frac{\Gamma(0.5, z_1^2 x / (2\delta^2))}{\Gamma(0.5)} \end{aligned} \quad (14)$$

As noted before, the corner point  $z_0 \in (0, \infty)$  may be chosen arbitrarily, while  $z_1$  is fixed. Hence the lower bound may be optimised wrt  $z_0$  at each  $x$  value to obtain a tighter lower bound:

$$\max_{z_0 \in (0, \infty)} \left\{ \frac{2}{\pi H_0} \left( \left( \frac{z_0^2 x}{2\delta^2} \right)^{0.5-|\lambda|} \frac{\gamma(|\lambda|, z_0^2 x / (2\delta^2))}{\Gamma(0.5)} + \frac{\Gamma(0.5, z_0^2 x / (2\delta^2))}{\Gamma(0.5)} \right) \right\} \leq \rho(x)$$

The (numerically optimised) lower bound and (fixed) upper bound on the mean acceptance rate  $\rho(x)$  are visualised for different parameter settings in Fig. 4. It can be observed, as expected from the inequalities (14), that the bounds are tight as  $x \rightarrow 0$  and  $x \rightarrow \infty$ , and that acceptance rates get lower as  $|\lambda|$  increases. In all cases though they indicate that only large jumps (large  $x$  values) will be rejected, and that at some point all jumps below a certain  $x$  value are highly likely to be accepted on average.

### 3.2 Simulation of GIG processes with $|\lambda| < 0.5$

The simple bound of Theorem 3.1 cannot be straightforwardly applied to simulation the GIG process for  $|\lambda| < 0.5$ . Instead we use the more sophisticated piecewise bounds of Theorem 3.2 and Corollary 3.2.1, which give us the dominating point process (13) that can be split into two independent point processes  $N_1$  and  $N_2$  as follows:

$$N_1 : \frac{e^{-x\gamma^2/2} (2\delta^2)^{|\lambda|} \gamma(|\lambda|, z_0^2 x / (2\delta^2)) \frac{\Gamma(|\lambda|) \sqrt{\text{Ga}}(z || \lambda |, x / (2\delta^2))}{\gamma(|\lambda|, z_0^2 x / (2\delta^2))}}{\pi^2 x^{1+|\lambda|} H_0 z_0^{2|\lambda|-1}} \mathcal{I}_{z < z_0}$$

$$N_2 : \frac{e^{-x\gamma^2/2} (2\delta^2)^{0.5} \Gamma(0.5, z_0^2 x / (2\delta^2)) \frac{\Gamma(0.5) \sqrt{\text{Ga}}(z|0.5, x/(2\delta^2))}{\Gamma(0.5, z_0^2 x / (2\delta^2))}}{\pi^2 x^{3/2} H_0} \mathcal{I}_{z \geq z_0}$$

Each may be simulated using a thinned tempered stable process for  $x$  and a truncated  $\sqrt{\text{Ga}}$  density for  $z$ . Having simulated each pair  $(x, z)$  they are accepted with probability equal to the ratio  $Q_{GIG}(x, z) / Q_{GIG(x, z)}^0$ . Owing to the piecewise form of the acceptance probability the two processes may be treated independently, including accept reject steps and the point process union taken at the final step to achieve the final GIG samples.

The sampling recipe for point process  $N_1$  is:

1.  $N_1 = \emptyset$
2. Use the thinned series method to simulate points  $x_i, i = 1, \dots$  from a point process with intensity function:

$$\frac{e^{-x\gamma^2/2} (2\delta^2)^{|\lambda|} \gamma(|\lambda|, z_0^2 x / (2\delta^2))}{\pi^2 x^{1+|\lambda|} H_0 z_0^{2|\lambda|-1}}$$

which is a modified tempered  $|\lambda|$ -stable process, see Section 3.3 for details.

3. For each  $x_i$ , simulate a  $z_i$  from a truncated square-root gamma density:

$$\frac{\Gamma(|\lambda|) \sqrt{\text{Ga}}(z||\lambda|, x_i/(2\delta^2))}{\gamma(|\lambda|, z_0^2 x_i / (2\delta^2))} \mathcal{I}_{0 < z < z_0}$$

4. With probability

$$\frac{H_0}{|H_{|\lambda|}(z_i)|^2 \left( \frac{z_i^{2|\lambda|}}{z_0^{2|\lambda|-1}} \right)}$$

accept  $x_i$ , i.e. set  $N_1 = N_1 \cup x_i$ , otherwise discard  $x_i$ .

Similarly, for  $N_2$ , the sampling recipe for an independent point process is as follows:

1.  $N_2 = \emptyset$
2. Use the thinned series method to simulate points  $x_i, i = 1, \dots$  from a point process with intensity function:

$$\frac{e^{-x\gamma^2/2} (2\delta^2)^{0.5} \Gamma(0.5, z_0^2 x / (2\delta^2))}{\pi^2 x^{3/2} H_0}$$

3. For each  $x_i$ , simulate a  $z_i$  from a truncated square-root gamma density:

$$\frac{\Gamma(0.5) \sqrt{\text{Ga}}(z|0.5, x_i/(2\delta^2))}{\Gamma(0.5, z_0^2 x_i / (2\delta^2))} \mathcal{I}_{z \geq z_0}$$

4. With probability:

$$\frac{H_0}{z_i |H_{|\lambda|}(z_i)|^2}$$

accept  $x_i$ , i.e. set  $N_2 = N_2 \cup x_i$ , otherwise reject  $x_i$

Finally, the set  $N = N_1 \cup N_2$  is the series of points from the GIG point process (still neglecting the additional gamma process that is required for  $\lambda > 0$ ).

### 3.2.1 Acceptance Rates

Theorem 3.2 is used once again to find lower bounds on the expected acceptance rates. In this case the bound to apply is  $z|H_\lambda(z)|^2 \leq A(z)$ .

For  $N_1$  the average acceptance rate  $\rho_1(x)$  is

$$\rho_1(x) = E \left[ \frac{H_0}{|H_{|\lambda|}(z)|^2 \left( \frac{z^{2|\lambda|}}{z_0^{2|\lambda|-1}} \right)} \right] = \int_0^{z_0} \frac{\Gamma(|\lambda|) \sqrt{\text{Ga}}(z||\lambda|, x/(2\delta^2))}{\gamma(|\lambda|, z_0^2 x/(2\delta^2))} \frac{H_0}{z|H_{|\lambda|}(z)|^2} \left( \frac{z_0}{z} \right)^{2|\lambda|-1} dz$$

which may be lower bounded by substituting the bound  $z|H_\lambda(z)|^2 \leq A(z)$  from Theorem 3.2 and by direct integration to give:

$$\rho_1(x) \geq \frac{H_0 z_0^{2|\lambda|-1} \pi^2}{2^{2|\lambda|} \Gamma^2(|\lambda|)}$$

Similarly, for  $N_2$  the average acceptance rate  $\rho_2(x)$  is

$$\rho_2(x) = E \left[ \frac{H_0}{z|H_{|\lambda|}(z)|^2} \right] = \int_{z_0}^{\infty} \frac{\Gamma(0.5) \sqrt{\text{Ga}}(z|0.5, x/(2\delta^2))}{\Gamma(0.5, z_0^2 x/(2\delta^2))} \frac{H_0}{z|H_{|\lambda|}(z)|^2} dz$$

and again lower bounds are obtained by substituting  $z|H_\lambda(z)|^2 \leq A(z)$  from Theorem 3.2 and direct integration to give:

$$\rho_2(x) \geq \frac{\pi H_0}{2}$$

We note that both of these bounds are in fact independent of the value of  $x$ . If we use  $B(z)$  to obtain an upper bound on the acceptance rates  $\rho_1$  and  $\rho_2$ , both bounds are found to be 1, i.e. no useful information is gleaned from the upper bound.

## 3.3 Sampling from the marginal point process envelope

In steps 2 above we require simulation of the marginal point process for  $x$  in the dominating bivariate point process. For  $N_1$  this has intensity:

$$Q_1(x) = \frac{e^{-x\gamma^2/2}}{\pi^2 x^{1+|\lambda|}} \frac{(2\delta^2)^{|\lambda|} \gamma(|\lambda|, z_0^2 x/(2\delta^2))}{H_0 z_0^{2|\lambda|-1}} = \frac{e^{-x\gamma^2/2}}{\pi^2 x} \frac{\gamma(|\lambda|, z_0^2 x/(2\delta^2))}{(z_0^2 x/(2\delta^2))^{|\lambda|} H_0 z_0^{-1}} \quad (15)$$

and we propose two possible methods for simulating this point process.

The first and most basic method uses the fact that the lower incomplete gamma function is upper bounded by the complete gamma function, i.e.  $\gamma(|\lambda|, z_0^2 x/(2\delta^2)) \leq \Gamma(|\lambda|)$ , which allows generation from  $Q_1$  by thinning of a tempered stable process. We thus have the following upper bounding envelope as a tempered stable density:

$$Q_1(x) \leq \bar{Q}_1^1(x) = \frac{e^{-x\gamma^2/2} \Gamma(|\lambda|)}{\pi^2 x^{1+|\lambda|}} \frac{(2\delta^2)^{|\lambda|}}{H_0 z_0^{2|\lambda|-1}}$$

This process may be routinely sampled by thinning of a positive tempered  $|\lambda|$ -stable process as described in 2.1.

Having generated points from the tempered stable envelope function the process is thinned with probability:

$$\frac{Q_1(x)}{\bar{Q}_1^1(x)} = \frac{\gamma(|\lambda|, z_0^2 x/(2\delta^2))}{\Gamma(|\lambda|)}$$

Experimentally we found that the acceptance rates were quite low for this bound, meaning that fairly long tempered stable series had to be generated (but see note below about the case  $\gamma = 0$ ), so a more sophisticated bound was sought, as follows.

The second and more effective method employs the following bound on the lower incomplete gamma function ([53], Theorem 4.1):

$$\frac{a\gamma(a, x)}{x^a} \leq \frac{(1 + ae^{-x})}{(a + 1)}$$

and so

$$\frac{\gamma(|\lambda|, z_0^2 x / (2\delta^2))}{(z_0^2 x / (2\delta^2))^{\lambda}} \leq \frac{(1 + |\lambda| e^{-z_0^2 x / (2\delta^2)})}{|\lambda|(|\lambda| + 1)} \quad (16)$$

so that the point process intensity function is upper bounded by

$$Q_1(x) \leq \bar{Q}_1^2(x) = \frac{e^{-x\gamma^2/2}}{\pi^2 x} \frac{z_0(1 + |\lambda| e^{-z_0^2 x / (2\delta^2)})}{|\lambda|(1 + |\lambda|)H_0}$$

Note that this is the intensity function of the union of two gamma processes, which may routinely be simulated using the methods of [33]. Specifically, the first gamma process has a shape parameter  $a_1 = \frac{z_0}{\pi^2 |\lambda| (1 + |\lambda|) H_0}$  and a rate parameter  $\beta_1 = \frac{\gamma^2}{2}$ . The second gamma process has a shape parameter  $a_2 = \frac{z_0}{\pi^2 (1 + |\lambda|) H_0}$  and a rate parameter  $\beta_2 = \frac{z_0^2}{(2\delta^2)} + \frac{\gamma^2}{2}$ . We can simulate these two gamma processes independently and their union will be thinned according to the following probability:

$$\frac{Q_1(x)}{\bar{Q}_1^2(x)} = \frac{|\lambda|(1 + |\lambda|)\gamma(|\lambda|, z_0^2 x / (2\delta^2))}{\left(\frac{z_0^2 x}{2\delta^2}\right)^{|\lambda|} (1 + |\lambda| e^{-z_0^2 x / (2\delta^2)})} \geq \frac{(1 + |\lambda|)e^{-|\lambda| \frac{z_0^2 x}{2\delta^2(1+|\lambda|)}}}{(1 + |\lambda| e^{-z_0^2 x / (2\delta^2)})}$$

Note that this method does not work for  $\gamma = 0$  since the underlying point process cannot be simulated in this case; instead the first method with bound  $\bar{Q}_1^1(x)$  must be used for the  $\gamma = 0$  case.

The second method for simulating  $N_1$ , using bounding function  $\bar{Q}_1^2(x)$ , is regarded as the superior approach for all parameter settings except for  $\gamma = 0$  since it has increased acceptance probabilities and also relies on an underpinning Gamma process rather than a  $|\lambda|$ -stable process as its basis, and the series representation of the Gamma process is known to converge very rapidly to zero compared to the  $|\lambda|$ -stable process [33], [39].

Similarly, for  $N_2$  we follow a thinning approach. The Lévy density for  $N_2$  is:

$$Q_2(x) = \frac{e^{-x\gamma^2/2}}{\pi^2 x^{3/2}} \frac{(2\delta^2)^{0.5} \Gamma(0.5, z_0^2 x / (2\delta^2))}{H_0} \quad (17)$$

Using the complete gamma function as part of an upper bound for this density, we can sample  $N_2$  as a tempered stable intensity  $\frac{e^{-x\gamma^2/2} (2\delta^2)^{0.5} \Gamma(0.5)}{\pi^2 H_0 x^{3/2}}$ , and apply thinning with probability  $\Gamma(0.5, z_0^2 x / (2\delta^2)) / \Gamma(0.5)$ . This is found to work well, but the rejection rates can be improved by more tightly upper bounding the term  $\Gamma(0.5, z_0^2 x / (2\delta^2))$ . The following simple bound is suitable, and valid for  $0 < s < 1$ :

$$\Gamma(s, x) \leq x^{s-1} e^{-x}$$

Using this bound we can write

$$\Gamma(0.5, z_0^2 x / (2\delta^2)) \leq (z_0^2 x / (2\delta^2))^{-1/2} e^{-z_0^2 x / (2\delta^2)} \quad (18)$$

so that the point process  $N_2$ 's intensity function is upper bounded by:

$$Q_2(x) \leq \bar{Q}_2(x) = \frac{(2\delta^2) e^{-\frac{x}{2} (\gamma^2 + z_0^2 / \delta^2)}}{\pi^2 x^2 z_0 H_0}$$

which is a tempered stable process and the thinning probability is:

$$\frac{Q_2(x)}{\bar{Q}_2(x)} = \frac{z_0 x^{0.5} \Gamma(0.5, z_0^2 x / (2\delta^2))}{(2\delta^2)^{0.5} e^{-z_0^2 x / (2\delta^2)}}$$

## 4 Simulations

In this section example simulations from the new method are generated and compared with a random variable generator for the GIG distribution [54], [55]. In the shot noise case 1000 terms are generated for each point process series representation and  $10^6$  random realisations are generated to produce Figs. 5-11, in which examples of the principal parameter ranges and edge case  $\gamma = 0$  are presented. In Figs. 12-15 example pathwise simulations are plotted for several parameter settings, drawing 30 independent realisations of the GIG process in each case. For cases where  $\lambda > 0$  the additional term in the Lévy density,  $\frac{e^{-x\gamma^2/2}}{x}$ , is generated as an independent Gamma process and the union of the these points with those from  $Q_{GIG}$  is taken to generate the final simulated process.

## 5 Discussion

This paper has presented a generic simulation methodology for GIG processes. The methods are simple and efficient to implement and have good acceptance rates, which will make them of use in applications for practitioners. Moreover, we provide code in Matlab and Python in order to give researchers immediate access to the methods.

Simulation of GIG processes opens up the possibility of simulation and inference for many more complex processes; in particular, a direct extension takes the sampled GIG process and generates other processes within the generalised shot-noise methodology [33]:

$$W(t) = \sum_{i=1}^{\infty} H(U_i, \Gamma_i) \mathcal{I}(V_i \leq t)$$

where  $U_i$  are iid uniform random variates and  $H(u, \gamma)$  a non-increasing function of  $\gamma$ . Of particular interest will be the mean-variance mixture of Gaussians, with:

$$H(U, \gamma) \sim \mathcal{N}(\mu_W h(\gamma), \sigma_W^2 h(\gamma))$$

and  $J_i = h(\Gamma_i)$  is the  $i$ th ordered jump of the simulated GIG process. This approach, which is an exactly equivalent process to the time-changed Brownian motion description of [37], leads directly to a simulation method for the Generalised Hyperbolic (GH) process, and its conditionally Gaussian form will enable inference for these processes, using a conditionally Gaussian approach similar in spirit to [34], [36]. Our continued work on these processes will study these inferential approaches with the GIG/GH model and also their use as driving processes for stochastic differential equations, again extending the approach of [36] to these more general classes of process.

## References

- [1] J. Bertoin, *Lévy Processes*, ser. Cambridge Tracts in Mathematics, 121. Cambridge University Press, 1997.
- [2] O. Barndorff-Nielsen, T. Mikosch, and S. Resnick, *Lévy Processes: Theory and Applications*. Birkhäuser Boston, 2001.
- [3] D. Applebaum, *Lévy Processes and Stochastic Calculus*, 2nd ed., ser. Cambridge Studies in Advanced Mathematics. Cambridge University Press, 2009. DOI: [10.1017/CBO9780511809781](https://doi.org/10.1017/CBO9780511809781).
- [4] B. Mandelbrot, “New methods in statistical economics,” *Journal of Political Economy*, vol. 71, no. 5, pp. 421–440, 1963.
- [5] E. F. Fama, “The behavior of stock-market prices,” *The Journal of Business*, vol. 38, no. 1, pp. 34–105, 1965.
- [6] R. Cont and P. Tankov, *Financial Modelling with Jump Processes*. Chapman & Hall/CRC, 2003.
- [7] N. Azzaoui and L. Clavier, “Statistical channel model based on  $\alpha$ -stable random processes and application to the 60 GHz ultra wide band channel,” *IEEE Transactions on Communications*, vol. 58, no. 5, pp. 1457–1467, May 2010.
- [8] J. Fahs and I. Abou-Faycal, “On the capacity of additive white alpha-stable noise channels,” in *2012 IEEE International Symposium on Information Theory Proceedings*, IEEE, 2012, pp. 294–298.
- [9] M. L. de Freitas, M. Egan, L. Clavier, A. Gouplil, G. W. Peters, and N. Azzaoui, “Capacity Bounds for Additive Symmetric  $\alpha$ -Stable Noise Channels,” *IEEE Transactions on Information Theory*, vol. 63, pp. 5115–5123, 2017.

- [10] J. Liebeherr and A. Burchard and F. Ciucu, "Delay bounds in communication networks with heavy-tailed and self-similar traffic," *IEEE Transactions on Information Theory*, vol. 58, no. 2, pp. 1010–1024, Feb. 2012.
- [11] G. Shevlyakov and K. Kim, "Robust minimax detection of a weak signal in noise with a bounded variance and density value at the center of symmetry," *IEEE Transactions on Information Theory*, vol. 52, no. 3, pp. 1206–1211, Mar. 2006.
- [12] D. J. Warren and J. B. Thomas, "Asymptotically robust detection and estimation for very heavy-tailed noise," *IEEE Transactions on Information Theory*, vol. 37, no. 3, pp. 475–481, May 1991.
- [13] C. L. Nikias and M. Shao, *Signal processing with alpha-stable distributions and applications*, ser. Adaptive and Learning Systems for Signal Processing, Communications, and Control. Wiley, 1995.
- [14] A. Achim, A. Bezerianos, and P. Tsakalides, "Novel Bayesian multiscale method for speckle removal in medical ultrasound images," *IEEE Transactions on Medical Imaging*, vol. 20, no. 8, pp. 772–783, Aug. 2001.
- [15] A. Achim, E. E. Kuruoğlu, and J. Zerubia, "SAR image filtering based on the heavy-tailed Rayleigh model," *IEEE Transactions on Image Processing*, vol. 15, no. 9, pp. 2686–2693, 2006.
- [16] S. Godsill and P. Rayner, "Statistical reconstruction and analysis of autoregressive signals in impulsive noise using the Gibbs sampler," *IEEE Transactions on Speech and Audio Processing*, vol. 6, no. 4, pp. 352–372, 1998. DOI: [10.1109/89.701365](https://doi.org/10.1109/89.701365).
- [17] M. J. Lombardi and S. J. Godsill, "On-line Bayesian estimation of signals in symmetric  $\alpha$ -stable noise," *Signal Processing, IEEE Transactions on*, vol. 54, no. 2, pp. 775–779, 2006.
- [18] R. W. Katz and B. G. Brown, "Extreme events in a changing climate: Variability is more important than averages," *Climatic Change*, vol. 21, no. 3, pp. 289–302, 1992.
- [19] R. W. Katz, M. B. Parlange, and P. Naveau, "Statistics of extremes in hydrology," *Advances in Water Resources*, vol. 25, no. 8–12, pp. 1287–1304, 2002.
- [20] X. Chen, Z. J. Wang, and M. J. McKeown, "Asymptotic analysis of robust lassos in the presence of noise with large variance," *IEEE Transactions on Information Theory*, vol. 56, no. 10, pp. 5131–5149, Oct. 2010.
- [21] M. Unser, P. Tafti, A. Amini, and H. Kirshner, "A unified formulation of Gaussian versus sparse stochastic processes - 2014; Part II: Discrete-domain theory," *IEEE Transactions on Information Theory*, vol. 60, no. 5, pp. 3036–3051, May 2014.
- [22] M. Unser, P. Tafti, and Q. Sun, "A unified formulation of Gaussian versus sparse stochastic processes - 2014; Part I: Continuous-domain theory," *IEEE Transactions on Information Theory*, vol. 60, no. 3, pp. 1945–1962, Mar. 2014, ISSN: 0018-9448.
- [23] M. Unser and P. D. Tafti, *An Introduction to Sparse Stochastic Processes*. Cambridge University Press, 2014.
- [24] A. Amini and M. Unser, "Sparsity and infinite divisibility," *IEEE Transactions on Information Theory*, vol. 60, no. 4, pp. 2346–2358, Apr. 2014.
- [25] R. E. Carrillo, A. B. Ramirez, G. R. Arce, K. E. Barner, and B. M. Sadler, "Robust compressive sensing of sparse signals: A review," *EURASIP Journal on Advances in Signal Processing*, vol. 2016, no. 1, p. 108, Oct. 2016.
- [26] M. E. Lopes, "Unknown sparsity in compressed sensing: Denoising and inference," *IEEE Transactions on Information Theory*, vol. 62, no. 9, pp. 5145–5166, Sep. 2016.
- [27] Z. Zhou and J. Yu, "Estimation of block sparsity in compressive sensing," *arXiv preprint arXiv:1701.01055*, 2017.
- [28] G. Tzagkarakis, "Bayesian Compressed Sensing Using  $\alpha$ -stable Distributions," Ph.D. dissertation, Department of Computer Science, University of Crete, Crete, Greece, 2009.
- [29] A. Achim, B. Buxton, G. Tzagkarakis, and P. Tsakalides, "Compressive sensing for ultrasound RF echoes using  $\alpha$ -Stable Distributions," in *2010 Annual International Conference of the IEEE Engineering in Medicine and Biology*, Aug. 2010, pp. 4304–4307.
- [30] E. Eberlein and E. A. v. Hammerstein, "Generalized hyperbolic and inverse Gaussian distributions: Limiting cases and approximation of processes," in *Seminar on Stochastic Analysis, Random Fields and Applications IV*, R. C. Dalang, M. Dozzi, and F. Russo, Eds., Basel: Birkhäuser Basel, 2004, pp. 221–264, ISBN: 978-3-0348-7943-9.

[31] E. Eberlein, “Application of generalized hyperbolic Lévy motions to finance,” in *Lévy Processes*, O. Barndorff-Nielsen, S. Resnick, and T. Mikosch, Eds., Birkhäuser, Boston, MA, 2001.

[32] A. Shah, A. Wilson, and Z. Ghahramani, “Student-t Processes as Alternatives to Gaussian Processes,” in *Proceedings of the Seventeenth International Conference on Artificial Intelligence and Statistics*, S. Kaski and J. Corander, Eds., ser. Proceedings of Machine Learning Research, vol. 33, Reykjavik, Iceland: PMLR, Apr. 2014, pp. 877–885. [Online]. Available: <http://proceedings.mlr.press/v33/shah14.html>.

[33] J. Rosiński, “Series representations of lévy processes from the perspective of point processes,” in *Lévy Processes: Theory and Applications*, O. E. Barndorff-Nielsen, S. I. Resnick, and T. Mikosch, Eds. Boston, MA: Birkhäuser Boston, 2001, pp. 401–415, ISBN: 978-1-4612-0197-7. doi: [10.1007/978-1-4612-0197-7\\_18](https://doi.org/10.1007/978-1-4612-0197-7_18). [Online]. Available: [https://doi.org/10.1007/978-1-4612-0197-7\\_18](https://doi.org/10.1007/978-1-4612-0197-7_18).

[34] T. Lemke and S. Godsill, “Inference for models with asymmetric  $\alpha$ -stable noise processes,” in *Unobserved Components and Time Series Econometrics*. : Oxford University Press, 2015, ch. 9.

[35] M. Riabiz, T. Ardeshiri, I. Kontoyiannis, and S. Godsill, “Nonasymptotic Gaussian approximation for inference with stable noise,” *IEEE Transactions on Information Theory*, vol. PP, pp. 1–1, May 2020. doi: [10.1109/TIT.2020.2996135](https://doi.org/10.1109/TIT.2020.2996135).

[36] S. Godsill, M. Riabiz, and I. Kontoyiannis, “The Lévy state space model,” in *2019 53rd Asilomar Conference on Signals, Systems, and Computers*, 2019, pp. 487–494. doi: [10.1109/IEEECONF44664.2019.9048715](https://doi.org/10.1109/IEEECONF44664.2019.9048715). eprint: <https://arxiv.org/abs/1912.12524>.

[37] O. E. Barndorff-Nielsen, “Processes of normal inverse Gaussian type,” *Finance and Stochastics*, vol. 2, no. 1, pp. 41–68, 1997. [Online]. Available: <https://ideas.repec.org/a/spr/finsto/v2y1997i1p41-68.html>.

[38] T. H. Rydberg, “The normal inverse Gaussian Lévy process: Simulation and approximation,” *Communications in Statistics. Stochastic Models*, vol. 13, no. 4, pp. 887–910, 1997. doi: [10.1080/15326349708807456](https://doi.org/10.1080/15326349708807456). [Online]. Available: <https://doi.org/10.1080/15326349708807456>.

[39] O. E. Barndorff-Nielsen and N. Shephard, “Non-Gaussian Ornstein–Uhlenbeck-based models and some of their uses in financial economics,” *Journal of the Royal Statistical Society: Series B (Statistical Methodology)*, vol. 63, no. 2, pp. 167–241, 2001. doi: <https://doi.org/10.1111/1467-9868.00282>. eprint: <https://rss.onlinelibrary.wiley.com/doi/pdf/10.1111/1467-9868.00282>. [Online]. Available: <https://rss.onlinelibrary.wiley.com/doi/abs/10.1111/1467-9868.00282>.

[40] S. Zhang, “Transition law-based simulation of generalized inverse Gaussian Ornstein–Uhlenbeck processes,” *Methodology and Computing in Applied Probability*, vol. 13, pp. 619–656, Sep. 2011. doi: [10.1007/s11009-010-9179-6](https://doi.org/10.1007/s11009-010-9179-6).

[41] S. Zhang, “Exact simulation of tempered stable Ornstein–Uhlenbeck processes,” *Journal of Statistical Computation and Simulation*, vol. 81, no. 11, pp. 1533–1544, 2011. doi: [10.1080/00949655.2010.494247](https://doi.org/10.1080/00949655.2010.494247). eprint: <https://doi.org/10.1080/00949655.2010.494247>. [Online]. Available: <https://doi.org/10.1080/00949655.2010.494247>.

[42] Y. Qu, A. Dassios, and H. Zhao, “Exact simulation of Ornstein–Uhlenbeck tempered stable processes,” *Journal of Applied Probability*, 2021.

[43] O. Barndorff-Nielsen and C. Halgreen, “Infinite divisibility of the hyperbolic and generalized inverse Gaussian distributions,” *Zeitschrift für Wahrscheinlichkeitstheorie und Verwandte Gebiete*, vol. 38, pp. 309–311, 1977.

[44] O. Kallenberg, *Foundations of Modern Probability*, 2nd. Springer-Verlag, 2002.

[45] T. S. Ferguson and M. J. Klass, “A Representation of Independent Increment Processes without Gaussian Components,” *The Annals of Mathematical Statistics*, vol. 43, no. 5, pp. 1634–1643, 1972. doi: [10.1214/aoms/1177692395](https://doi.org/10.1214/aoms/1177692395). [Online]. Available: <https://doi.org/10.1214/aoms/1177692395>.

[46] P. A. W. Lewis and G. S. Shedler, “Simulation of nonhomogeneous Poisson processes by thinning,” *Naval Research Logistics Quarterly*, vol. 26, no. 3, pp. 403–413, Sep. 1979. doi: [10.1002/nav.3800260304](https://doi.org/10.1002/nav.3800260304). [Online]. Available: <https://ideas.repec.org/a/wly/navlog/v26y1979i3p403-413.html>.

[47] N. Shephard and O. E. Barndorff-Nielsen, “Normal Modified Stable Processes,” University of Oxford, Department of Economics, Economics Series Working Papers 72, Jul. 2001. [Online]. Available: <https://ideas.repec.org/p/oxf/wpaper/72.html>.

[48] J. Rosiński, “Tempering stable processes,” *Stochastic Processes and their Applications*, vol. 117, no. 6, pp. 677–707, 2007, ISSN: 0304-4149. DOI: <https://doi.org/10.1016/j.spa.2006.10.003>. [Online]. Available: <https://www.sciencedirect.com/science/article/pii/S030441490600144X>.

[49] G. Samorodnitsky and M. S. Taqqu, *Stable non-Gaussian random processes : stochastic models with infinite variance*. CRC Press, 1994.

[50] R. Wolpert and K. Ickstadt, “Poisson/gamma random field models for spatial statistics,” *Biometrika*, vol. 85, no. 2, pp. 251–267, Jun. 1998, ISSN: 0006-3444. DOI: [10.1093/biomet/85.2.251](https://doi.org/10.1093/biomet/85.2.251). eprint: <https://academic.oup.com/biomet/article-pdf/85/2/251/846445/85-2-251.pdf>. [Online]. Available: <https://doi.org/10.1093/biomet/85.2.251>.

[51] P. Freitas, “Sharp bounds for the modulus and phase of Hankel functions with applications to Jaeger integrals,” *Math. Comput.*, vol. 87, pp. 289–308, 2018.

[52] G. Watson, *A Treatise on the Theory of Bessel Functions. 2nd Ed.* Cambridge University Press, 1944.

[53] E. Neuman, “Inequalities and bounds for the incomplete gamma function,” *Results in Mathematics*, vol. 63, Jun. 2013. DOI: [10.1007/s00025-012-0263-9](https://doi.org/10.1007/s00025-012-0263-9).

[54] L. Devroye, “Random variate generation for the generalized inverse Gaussian distribution,” *Statistics and Computing*, vol. 24, pp. 239–246, 2014.

[55] Statovic, “Gigrnd(p, a, b, samplesize),” *MATLAB Central File Exchange*, 2017. [Online]. Available: <https://www.mathworks.com/matlabcentral/fileexchange/53594-gigrnd-p-a-b-samplesize>.

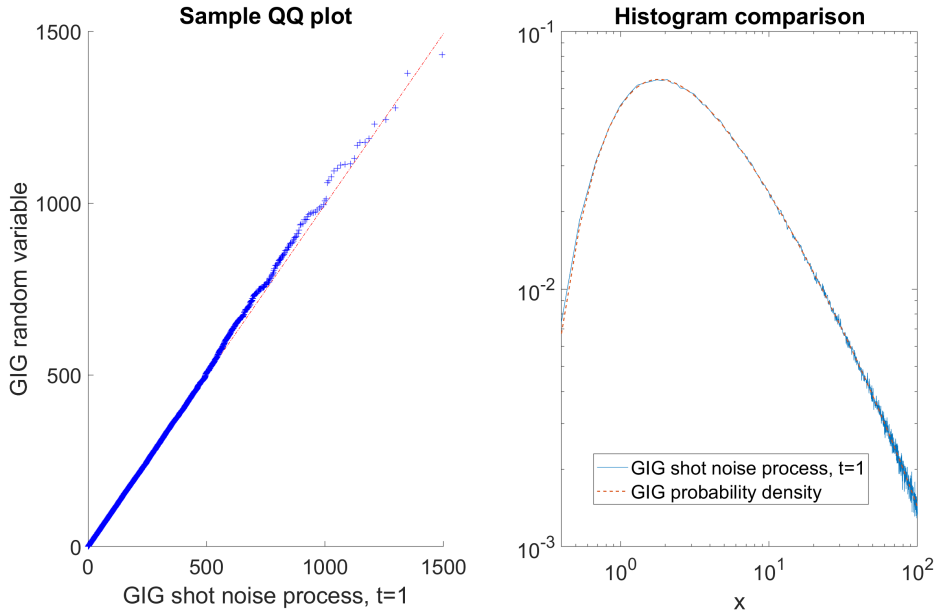


Figure 5: Simulation comparison between the shot noise generated GIG process and GIG random variates,  $\lambda = -0.1$ ,  $\gamma = 0.1$ ,  $\delta = 2$ ,  $10^6$  random samples.

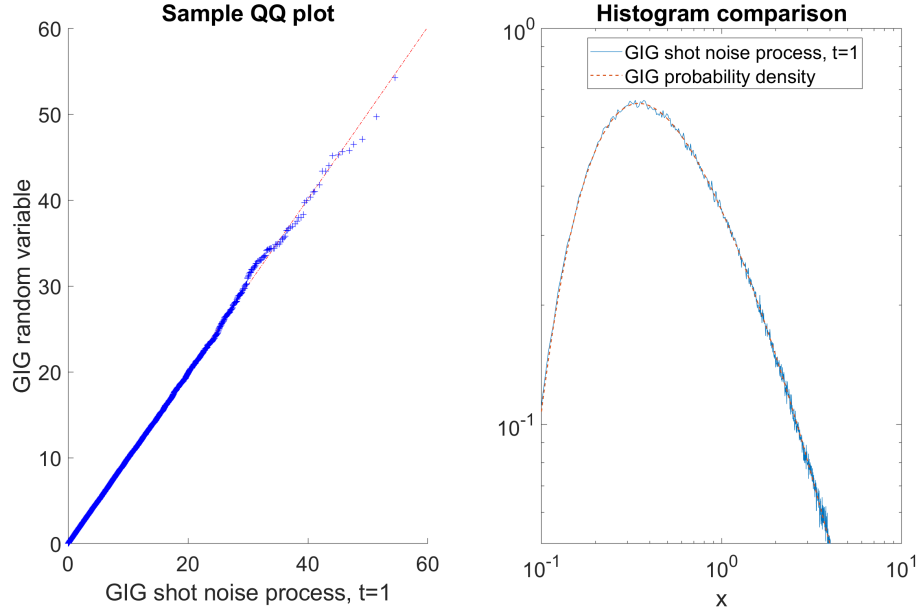


Figure 6: Simulation comparison between the shot noise generated GIG process and GIG random variates,  $\lambda = -0.4$ ,  $\gamma = 0.5$ ,  $\delta = 1$ ,  $10^6$  random samples.

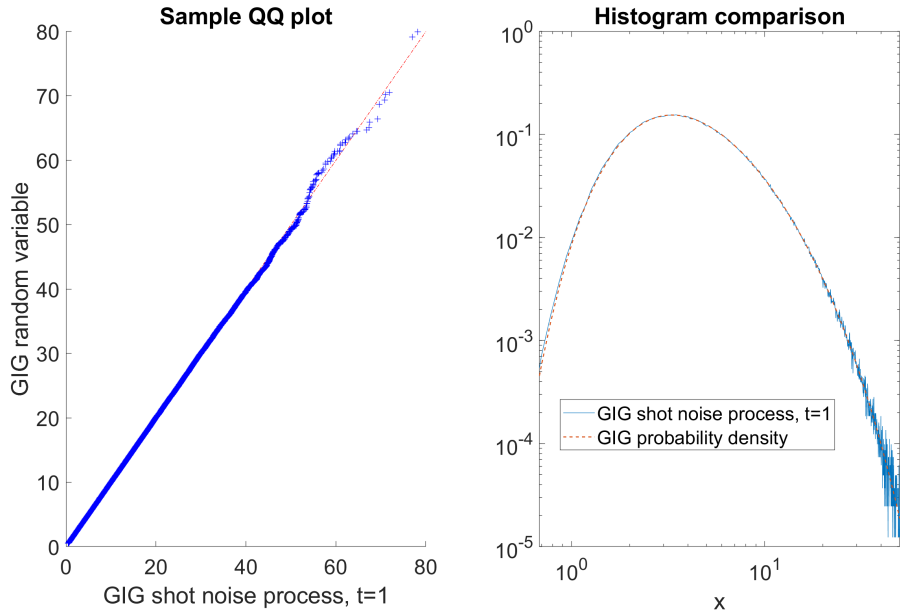


Figure 7: Simulation comparison between the shot noise generated GIG process and GIG random variates,  $\lambda = -1$ ,  $\gamma = 0.5$ ,  $\delta = 4$ ,  $10^6$  random samples.

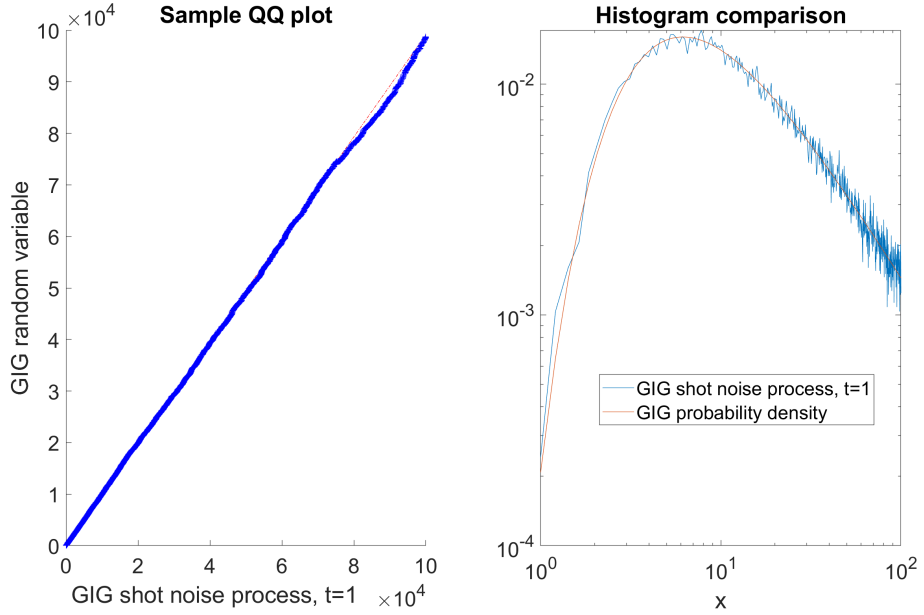


Figure 8: Simulation comparison between the shot noise generated GIG process and GIG random variates,  $\lambda = -0.3$ ,  $\gamma = 0$ ,  $\delta = 4$ ,  $10^6$  random samples.

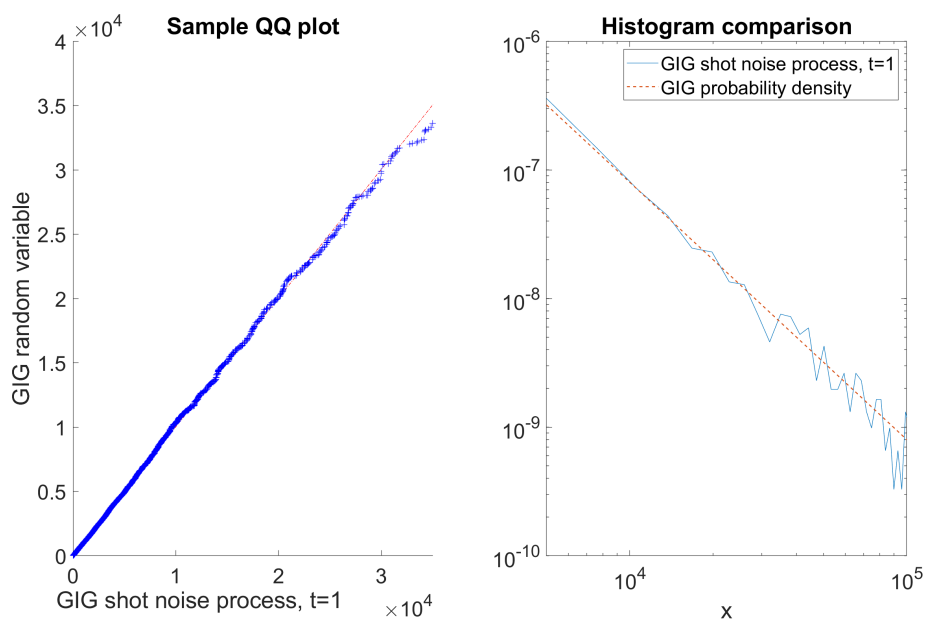


Figure 9: Simulation comparison between the shot noise generated GIG process and GIG random variates,  $\lambda = -1$ ,  $\gamma = 0$ ,  $\delta = 4$ ,  $10^6$  random samples.

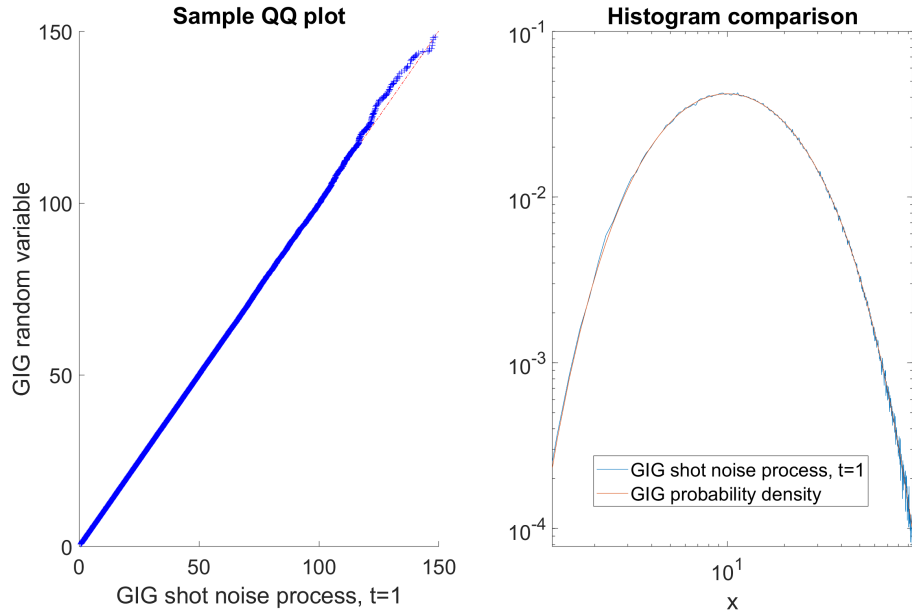


Figure 10: Simulation comparison between the shot noise generated GIG process and GIG random variates,  $\lambda = 1$ ,  $\gamma = 0.4$ ,  $\delta = 4$ ,  $10^6$  random samples.

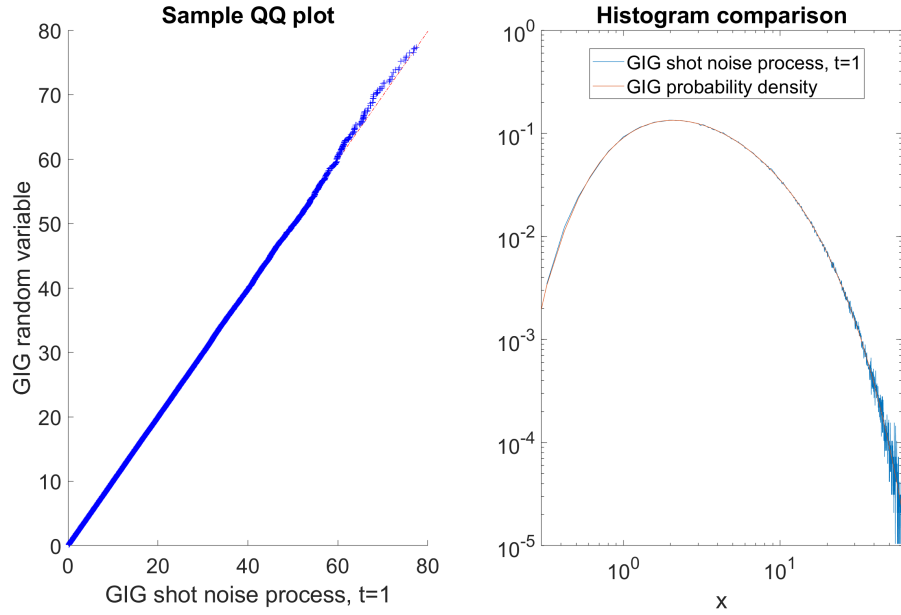


Figure 11: Simulation comparison between the shot noise generated GIG process and GIG random variates,  $\lambda = 0.3$ ,  $\gamma = 0.5$ ,  $\delta = 2$ ,  $10^6$  random samples.

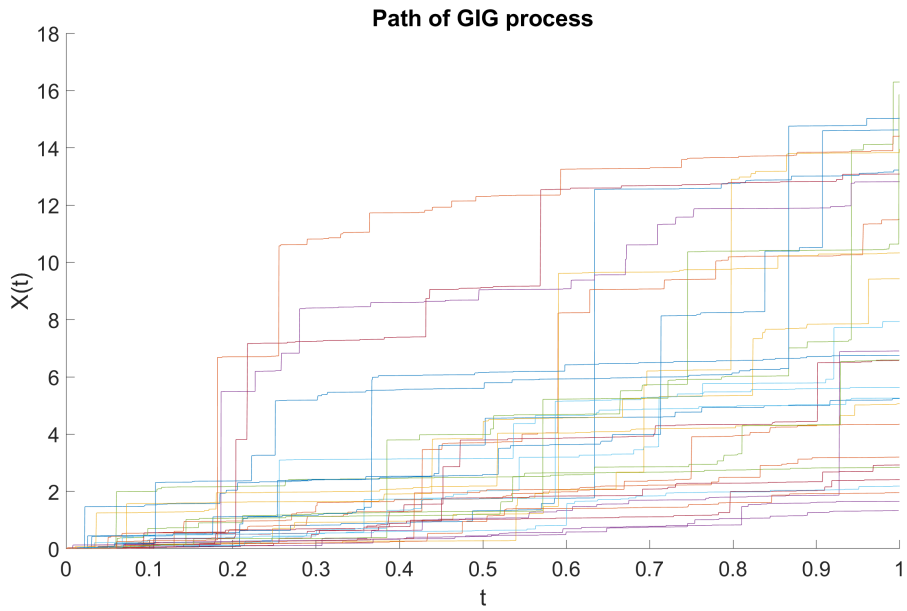


Figure 12: Pathwise simulations of the GIG process,  $\lambda = -0.1$ ,  $\gamma = 0.5$ ,  $\delta = 3$ .

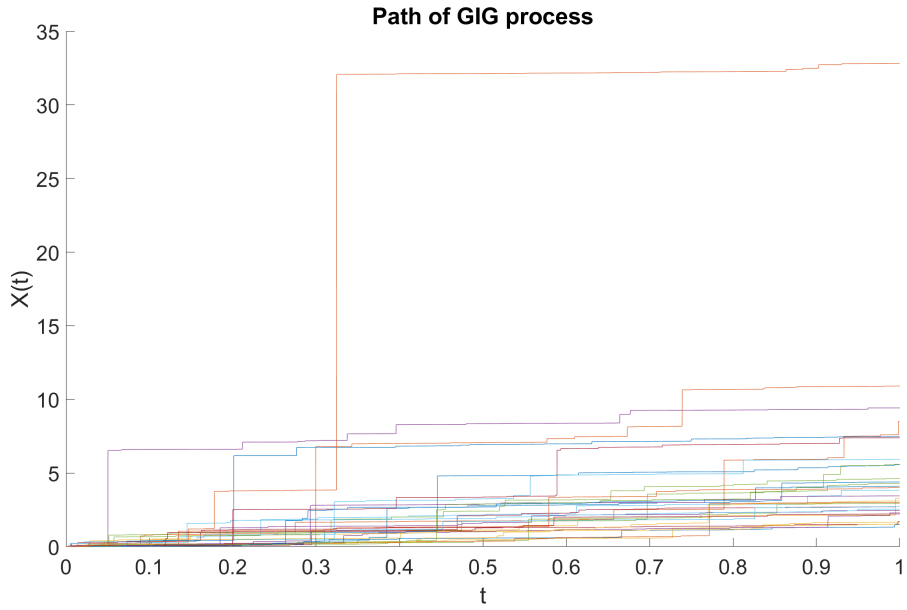


Figure 13: Pathwise simulations of the GIG process,  $\lambda = -1$ ,  $\gamma = 0.5$ ,  $\delta = 3$  (log-scale).

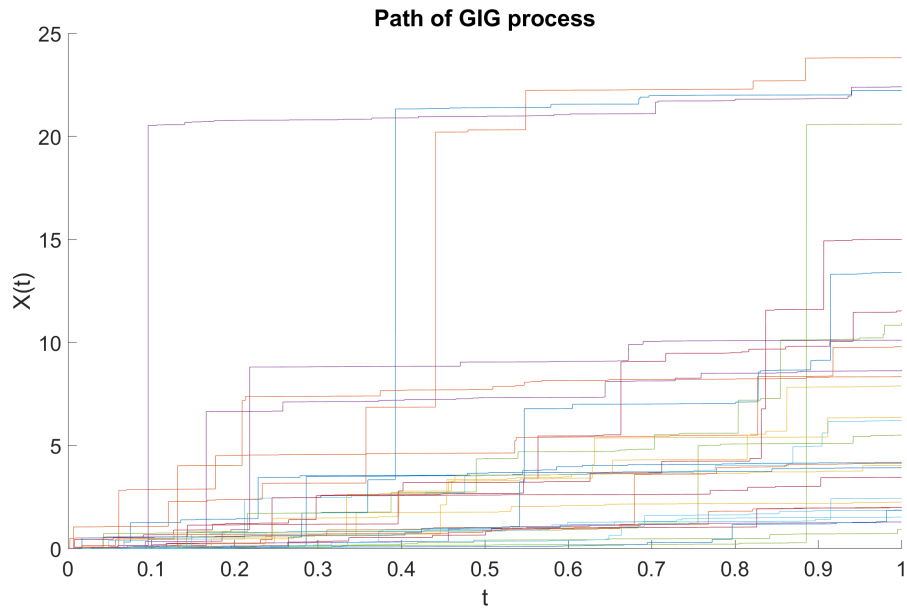


Figure 14: Pathwise simulations of the GIG process,  $\lambda = 1$ ,  $\gamma = 0.4$ ,  $\delta = 4$ .

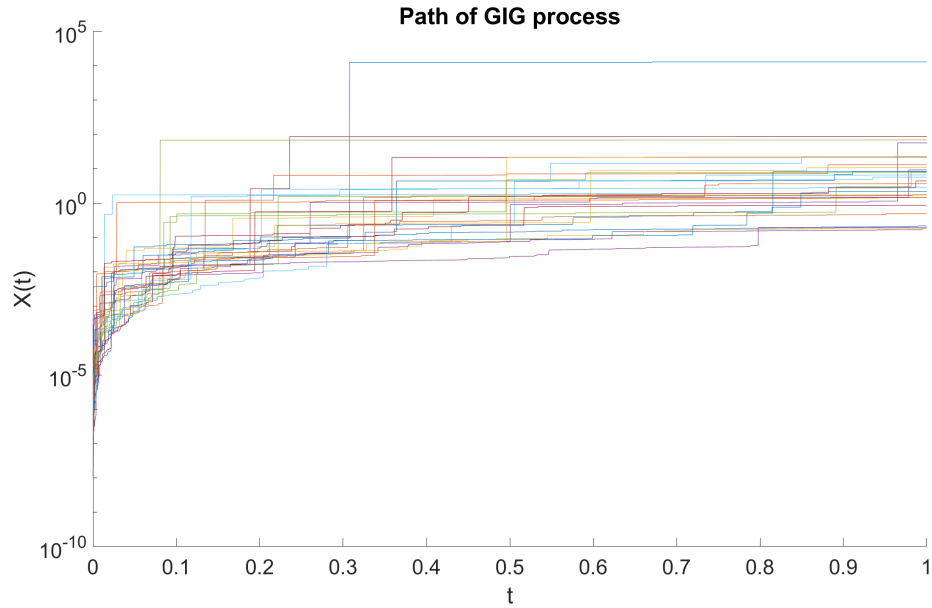


Figure 15: Pathwise simulations of the GIG process,  $\lambda = -0.4$ ,  $\gamma = 0$ ,  $\delta = 1$  (log-scale).